Environmental Science Processes & Impacts

PAPER

View Article Online
View Journal | View Issue

Cite this: *Environ. Sci.: Processes Impacts*, 2026, **28**, 1843

Measurement of octanol–air and air–water partition coefficients of isopropyl and isobutyl nitrate

Ariana J. Buss, Kevin D. Easterbrook, Van Khanh Le, Dmitry N. Ivanov, Nicole Sandblom and Hans D. Osthoff *

Received 13th November 2025
Accepted 23rd May 2026

DOI: 10.1039/d5em00940e

rsc.li/espi

This work provides the first experimental determination of Henry's law solubility constants ($H_S^{cp} \equiv H$) in *n*-octanol (H_{oct}) for isopropyl and isobutyl nitrate (IPN and IBN) over the 284.65 K to 309.65 K temperature (T) range. The H constants were measured by dynamic gas stripping using a bubble column apparatus and gas chromatography with electron capture detection (GC-ECD). The H_{oct} data are best described by $\ln(H_S^{cp}(IPN)_{oct}/[M\ atm^{-1}]) = -(10.60 \pm 1.54) + (4214 \pm 459)/T$ and $\ln(H_S^{cp}(IBN)_{oct}/[M\ atm^{-1}]) = -(12.01 \pm 0.85) + (4937 \pm 253)/T$, where T is in kelvin. In addition, their H constants in deionized water (H_{aq}) were measured to corroborate literature H_{aq} values. The H_{aq} and H_{oct} data were combined to calculate octanol–water partition coefficients ($K_{OW} = H_{oct}/H_{aq}$), obtaining average values of (33 ± 5) for IPN and (1.3 ± 0.1) × 10^2 for IBN. The experimental data were compared to predictions of H_{oct}, H_{aq} and K_{OW} by structure–activity relationship models (SARs).

Environmental significance

Isopropyl and isobutyl nitrate are notable nitrogen oxide (NO_x) reservoir species and significantly contribute to the redistribution of NO_x throughout the troposphere, impacting global budgets of ozone (O_3) and secondary organic aerosol (SOA). To correctly model their global distributions and hence their impact on atmospheric composition, accurate experimentally constrained parameterizations of their partitioning between gas, aqueous and organic phases are required. The phase partitioning of alkyl nitrates is generally understudied but needed to verify and improve the accuracy of structure–activity relationship model predictions of partition coefficients for organic nitrates that are not readily experimentally accessible, but which affect the global distribution of NO_x (such as isoprene or terpene nitrates).

1 Introduction

Alkyl nitrates (ANs; molecular formula $RONO_2$) are important trace gas constituents of the troposphere, the lowest layer of the atmosphere, where they constitute a significant component of "odd nitrogen" (NO_y). Because ANs sequester nitrogen oxides ($NO_x = NO + NO_2$), their chemistry affects the budgets of ozone (O_3) and secondary organic aerosol (SOA) as they undergo deposition, oxidation, photolysis, or incorporation into aerosol.[1–3] To correctly model the global distributions of ANs, accurate parameterizations for their partitioning between gas, aqueous and organic phases are required.

Atmospheric chemists commonly use Henry solubility in units of M atm^{-1} (H_S^{cp}, for simplicity referred to as H in this manuscript), which is defined as the ratio of liquid phase concentration (in M) over the partial pressure (in atm) of the gas. The dimensionless Henry solubility (H_S^{cc}) is related to H by

$$H_S^{cc} = H_S^{cp} RT = HRT \quad (1)$$

where R is the universal gas constant (~0.08205 L atm mol^{-1} K^{-1}), and T is the temperature in kelvin.[4]

For measurements in water, the dimensionless Henry solubility (*i.e.*, $H_S^{cc}(aq)$) describes the distribution of a molecule between the gas and aqueous phases at equilibrium.[4,5] This quantity is equal to the inverse of the air–water partition coefficient (K_{AW}), *i.e.*, equal to the water–air partition coefficient (K_{WA}). A related quantity is the octanol–air partition coefficient ($K_{OA} = H_S^{cc}(octanol)$), which describes the equilibrium distribution of a molecule between *n*-octanol and the vapour phase.[6] These two quantities are interconnected with the octanol–water partition coefficient (K_{OW}) *via* the triangular thermodynamic relationship:

$$K_{OW} = \frac{K_{OA}}{K_{WA}} = \frac{H_S^{cc}(octanol)}{H_S^{cc}(aq)} = \frac{H_S^{cp}(octanol)}{H_S^{cp}(aq)} \quad (2)$$

The octanol–water partition coefficient is a widely used parameter to estimate the hydrophobicity and partitioning of

Department of Chemistry, University of Calgary, 2500 University Drive N.W., Calgary, Alberta, Canada, T2N 1N4. E-mail: hosthoff@ucalgary.ca

Table 1 Experimental log(K_{OA}) and log(K_{OW}) values for selected organic nitrates at $T = 298$ K

Compound	CAS no.	log(K_{OA})	log(K_{OW})	Reference
1-Nitrooxy-2-propanol	20266-65-3	5.62 ± 0.03	0.26[a]	9
1-Nitrooxy-2-butanol	3156-74-9	5.83 ± 0.06	0.80[a]	9
4-(Nitrooxy)butan-2-ol	141299-18-5	6.23 ± 0.02	0.48[a]	9
4-(Nitrooxy)butan-1-ol	22911-39-3	6.91 ± 0.09	0.16[a]	9
5-Nitrooxy-2-pentanol	n/a	6.53 ± 0.06	0.82[a]	9
1,4-Butyl dinitrate	3457-91-8	4.61 ± 0.03	1.44[a]	9
n-Pentyl nitrate	1002-16-0	3.03 ± 0.04	2.70[a]	9
Peroxyacetic nitric anhydride (PAN)	2278-22-0	2.92 ± 0.02	1.07 ± 0.03	10
Peroxypropionic nitric anhydride (PPN)	5796-89-4	3.33 ± 0.02	1.77 ± 0.03	11
Ethyl nitrate (EN)	625-58-1	2.58 ± 0.04	1.00 ± 0.04	12
Isopropyl nitrate (IPN)	1712-64-7	2.936 ± 0.007	1.58 ± 0.01[b] 1.66 ± 0.01[c]	This work
Isobutyl nitrate (IBN)	543-29-3	3.38 ± 0.02	2.16 ± 0.02	This work

[a] Derived from the fragment constant estimation method developed by Hansch and Leo.[13] [b] Calculated using H_{aq} and H_{oct} values determined by this group. [c] Calculated using H_{aq} values from Kames and Schurath[14] and H_{oct} values determined by this group.

a molecule from water to organic media such as lipids, waxes, and natural organic matter, including organic aerosol.[7]

Despite the importance of ANs for atmospheric chemistry,[8] K_{OA} and K_{OW} values have been experimentally determined for only a few of them (Table 1). Experimentally derived octanol–air and octanol–water partition coefficients are particularly lacking for short-chain (C_1–C_5) ANs, which are typically the most abundant ANs found in the troposphere. In this regard, K_{OA} and K_{OW} values have to date only been reported for ethyl nitrate (EN)[12] and *n*-pentyl nitrate.[9] In addition, Treves *et al.*[9] reported K_{OA} and K_{OW} values for 1-nitrooxy-2-propanol, 1-nitrooxy-2-butanol, 4-(nitrooxy)butan-2-ol, 4-(nitrooxy)butan-1-ol, 5-nitrooxy-2-pentanol, and 1,4-butylene dinitrate, and Fischer and Ballschmiter[15,16] reported K_{OW} values for a series of alkyl dinitrates (not listed in Table 1).

Analogous measurements for peroxycarboxylic nitric anhydrides (PANs), another important class of organic nitrates, are also scarce. At present, K_{OA} and K_{OW} values have only been reported for the two most abundant PANs: peroxyacetic nitric anhydride (PAN) by Roberts[10] and peroxypropionic nitric anhydride (PPN) by Easterbrook *et al.*[11] (Table 1).

The paucity of literature on this topic is surprising considering that measurements of K_{OA} and K_{OW} for other types of molecules have been very comprehensive.[6] On the contrary, some compilations[17,18] have omitted organic nitrates as a molecular class altogether. This lack of experimental data hampers the ability to accurately predict, *e.g.*, *via* structure–activity relationship (SAR) models,[19] K_{OA} and K_{OW} values for organic nitrates, especially for molecules that are not readily experimentally accessible such as monoterpene-derived nitrates.[20]

To expand the data set of known K_{OA} and K_{OW} values for the alkyl nitrate chemical family, we measured K_{OA} for two commercially available ANs, 2-propyl nitrate (also referred to as isopropyl nitrate, IPN) and 2-methyl-1-propyl nitrate (also referred to as isobutyl nitrate, IBN), in *n*-octanol at T between 284.65 K and 309.65 K. These compounds are often the most abundant low molecular weight ANs in the lower troposphere.[21,22] Further, a recent laboratory study has shown that photolysis in aqueous droplets constitutes a significant sink for IPN and IBN,[23] resulting in renewed interest in quantifying their partitioning from the gas to the condensed phase at tropospherically relevant temperatures. We calculate K_{OW} values for IPN and IBN *via* eqn (2) using K_{OA} values measured in this work and K_{WA} values derived from the T-dependent H_{aq} parameterizations reported by Kames and Schurath,[14] which were verified *via* additional experiments in deionized (DI) water. Finally, we compare our results with model-predicted partition coefficients and discuss implications for the prediction of species for which limited experimental data are available.

2 Methods

Henry's law solubility and liquid-phase loss rate constants (beyond partitioning) were determined by inert gas stripping[24] using a jacketed, Pyrex bubble column apparatus as described previously.[11,12] The apparatus (Fig. S1) was temperature-controlled using an external chiller-circulator (Lauda Proline RP 1290) and connected to a gas chromatograph with electron capture detection (GC-ECD, model HP-5890)[25] using 1/8″ (~0.32 cm) outer diameter (o.d.) stainless steel tubing and fittings (Swagelok Ultra-Torr). The tubing spanning from the bubble column output to the GC-ECD was wrapped with a line heater (Watlow; labelled "heated sample line" in Fig. S1) and maintained at 60 °C *via* a benchtop temperature controller (Omega, model CSi32K-C24) and embedded K-type thermocouples (Omega). The GC was equipped with a 15 m long megabore column (Restek RTX-200, film thickness 1 μm) and a 50 μL stainless steel sample loop (VICI Cheminert) and was operated at an oven temperature of 60 °C, an ECD temperature of 150 °C, and with N_2 carrier and make-up gas (delivered from the blow-off of a liquid N_2 dewar) with typical flow rates of ~8.1 mL min^{-1} and ~80 mL min^{-1}, respectively. The GC injections were automated, with a new run starting every 10 min.

While the temperature of the chiller-circulator bath is accurate to ±0.01 °C, the blow-off from its internal fan slightly, yet systematically, affected the temperature of the liquid flowing through the jacket of the adjacent bubble column apparatus.

Temperatures reported here were corrected for this effect by measuring the temperature of the liquid exiting the jacket. For a bath set point of 281.65 K, for example, the actual temperature of the liquid exiting the jacket was 283.25 K.

In a typical experiment, the bubble column apparatus was filled with a known volume (V_l; measured using a graduated cylinder) of either *n*-octanol (ACS reagent grade, ≥99% purity, used as received) or DI water (18 MΩ cm^{-1}, Thermo Scientific Barnstead Nanopure Model D11931), to which small quantities of IPN (~1 drop; ≥99% manufacturer-specified purity) and IBN (~1–5 drops; ≥95.5%) were added using a glass pipette. Both compounds were purchased from Sigma-Aldrich and used as received; however, the production of IBN was discontinued before all planned experiments could be completed. For experiments with DI water, IBN was synthesized from the reaction of dinitrogen pentoxide (N_2O_5) with anhydrous 2-methyl-1-propanol (99.5% purity, used as received) as described by Kames *et al.*[26] Batches of N_2O_5 were synthesized in a linear flow tube by titrating nitric oxide (NO; >99%, Praxair) with excess O_3 (generated using an OzoneLab OL80F/T Ozone Generator) in dry O_2 gas (Air Liquide ALPHAGAZ 1) until the gas stream was colourless.[27,28] White N_2O_5 crystals were collected in a glass trap externally cooled with dry ice.

For experiments in *n*-octanol, N_2 gas (also from the liquid N_2 dewar blow-off) was delivered directly to the apparatus *via* a calibrated 500 standard (0 °C, 1 bar) cubic centimetre per minute (sccm) capacity mass flow controller (MFC, MKS Instruments) and bubbled through the liquid solution. To limit evaporative losses of the solvent in DI water experiments, the N_2 gas stream was humidified upstream from the main bubble column apparatus using a second bubbler containing DI water (not shown in Fig. S1). The temperature of the second bubbler was maintained below the setpoint of the main apparatus using a second recirculating chiller (VWR 1190S) to avoid condensation of water in the connecting tubing.

The gas-phase concentrations of IPN and IBN (c_g) were then monitored as a function of time (t) by GC-ECD. Sample chromatograms highlighting the decay of IPN and IBN peak areas as a function of t (and the absence of impurity peaks) are shown in Fig. 1. For the example shown, the GC-ECD sampled downstream from 150.0 mL of *n*-octanol at 298.65 K through which 537 mL min^{-1} N_2 gas was bubbled. The two compounds eluted the GC column at ~63.4 s (IPN) and ~98.4 s (IBN). The insert shows a full time series of the IPN and IBN decay profiles for this experiment, as well as enlarged diamond symbols that represent IPN and IBN peak areas derived from the chromatograms shown in the main figure. Their peak areas were determined by numerical integration using a custom macro in Igor Pro (Wavemetrics Inc.). The experiment was repeated, systematically varying the flow rate to volume ratio $\left(\frac{\Phi}{V_l}\right)$, as summarized in Tables S1–S3.

The concentration decays due to a combination of chemical reactions within the liquid phase and gas–liquid equilibration, *i.e.*, partitioning of IPN (or IBN) from the liquid reservoir to the gas stream. Kames and Schurath[29] showed that under

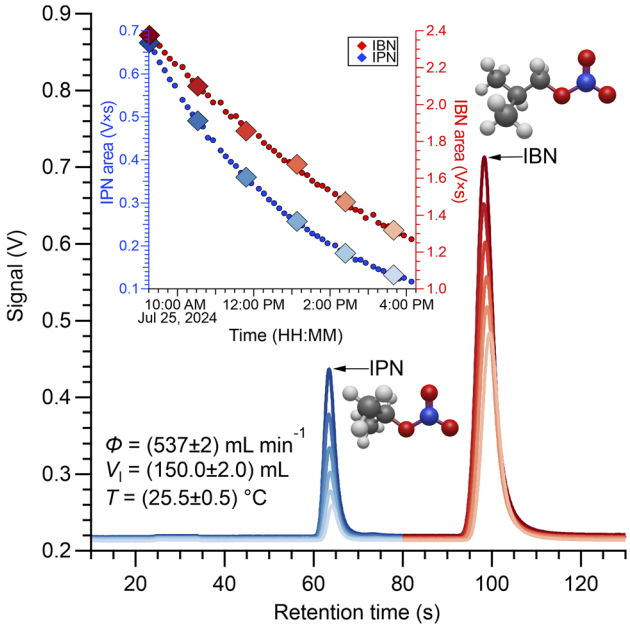

Fig. 1 Sample chromatograms recorded by the Hewlett Packard GC-ECD. Here, the GC sampled the gas stream eluting from 150.0 mL of *n*-octanol at a temperature of 298.65 K and a volumetric flow rate of 537 mL min^{-1}. Six chromatograms are shown to demonstrate the decay of IPN (blue colour) and IBN (red colour) over time, which were recorded at t = 0 min, 76 min, 152 min, 232 min, 308 min, and 384 min after IPN and IBN were added to the bubble column. The insert shows the full time series of the peak area decay for each compound, where the enlarged diamond symbols correspond to the chromatographic peaks shown in the main figure.

conditions of rapid gas–liquid equilibration, the analyte's concentration decreases according to the following relationship:

$$-\frac{\mathrm{d}}{\mathrm{d}t}c_{g,t} = \left(\frac{\Phi}{H_S^{cc}V_l} + k_l\right)c_{g,t} \quad (3)$$

Here, $c_{g,t}$ is the analyte's concentration in the gas-phase at time t and k_l is the loss rate constant of IPN (or IBN) in the liquid phase. Since the chromatographic peak area (A) is proportional to c_g,[30] integration of eqn (3) and substituting A for c_g yields:

$$\ln\left(\frac{c_{g,0}}{c_{g,t}}\right) = \ln\left(\frac{A_0}{A_t}\right) = \left(\frac{\Phi}{H_S^{cc}V_l} + k_l\right)t \quad (4)$$

Representative plots of $\ln\left(\frac{c_{g,0}}{c_{g,t}}\right)$ *versus* t for IPN and IBN at several N_2 gas flow rates (Φ) downstream from 150.0 mL of *n*-octanol at 298.65 K are shown in Fig. 2A and B, respectively. Plots such as those shown in Fig. 2 were linear for both IPN and IBN across all temperature conditions, with Pearson correlation coefficients (r) ≥ 0.972 (for IPN) and ≥0.911 (for IBN) (Table S1).

The observed linearity confirms a first order outgassing process, with higher flow rates leading to faster outgassing from the liquid reservoir. Experiments in DI water were linear over time, with r ≥ 0.996 for IPN and ≥0.988 for IBN (Tables S2 and S3).

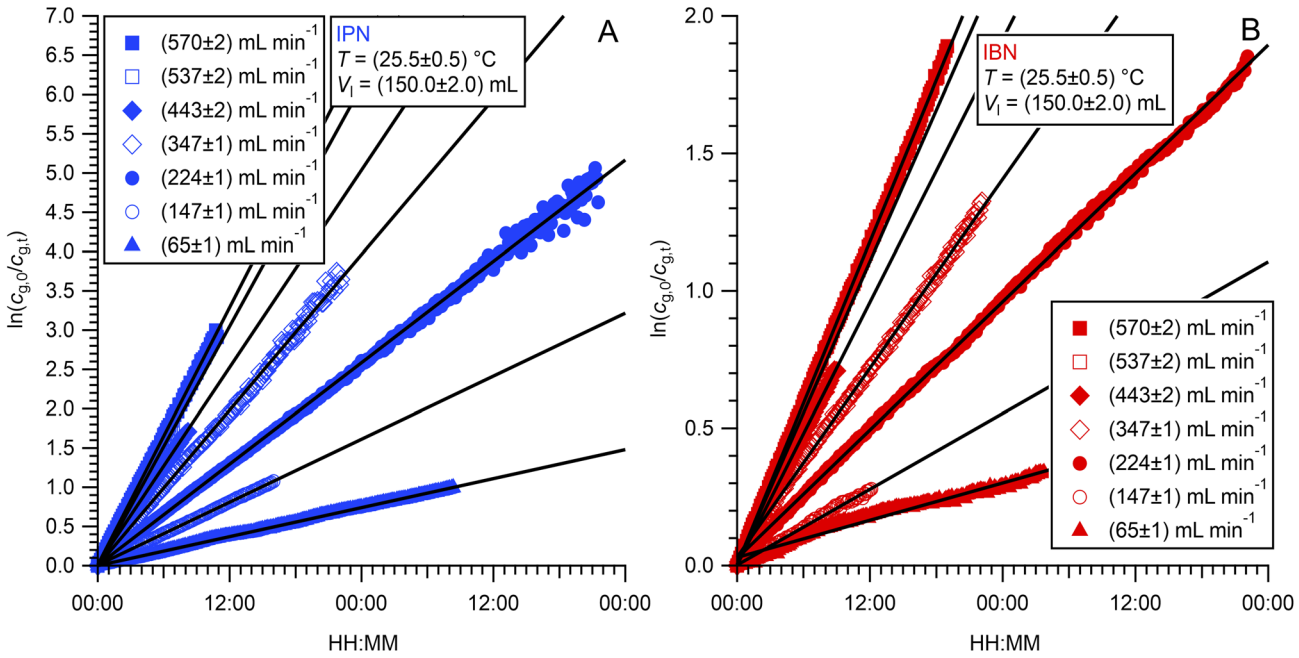

Fig. 2 Example plots of $\ln(c_{g,0}/c_{g,t})$ *versus* t for IPN (panel A, blue colour) and IBN (panel B, red colour) at seven different N_2 gas flow rate (*i.e.*, Φ) conditions. Reflected in the figure, both IPN and IBN were observed downstream from 150.0 mL of *n*-octanol at a temperature of 298.65 K. The solid black lines are linear fits to the data at each temperature.

Linear regression analysis of plots of $\frac{d}{dt}\ln\left(\frac{A_0}{A_t}\right)$ *versus* $\frac{\Phi}{V_l}$ then yields $\frac{1}{H_S^{cc}}$ as the slope and k_l as the ordinate (*i.e.*, *y*-intercept). Fig. 3 shows representative plots of $d\ln(c_{g,0}/c_{g,t})/dt$ as a function of $\frac{\Phi}{V_l}$ for IPN (Fig. 3A) and IBN (Fig. 3B) in *n*-octanol at temperatures of 309.65 K, 304.95 K, 298.65 K, 293.85 K, and 284.65 K. Analogous plots for experiments in DI water are shown in Fig. S2A (IPN) and S2B (IBN). The fit results and resulting values of H_S^{cc} for IPN and IBN are summarized in Tables S4 and S5. For each T, H_S^{cp} constants (H_{oct} for *n*-octanol and H_{aq} for DI water) for IPN and IBN were then calculated from measured H_S^{cc} values *via* eqn (1).

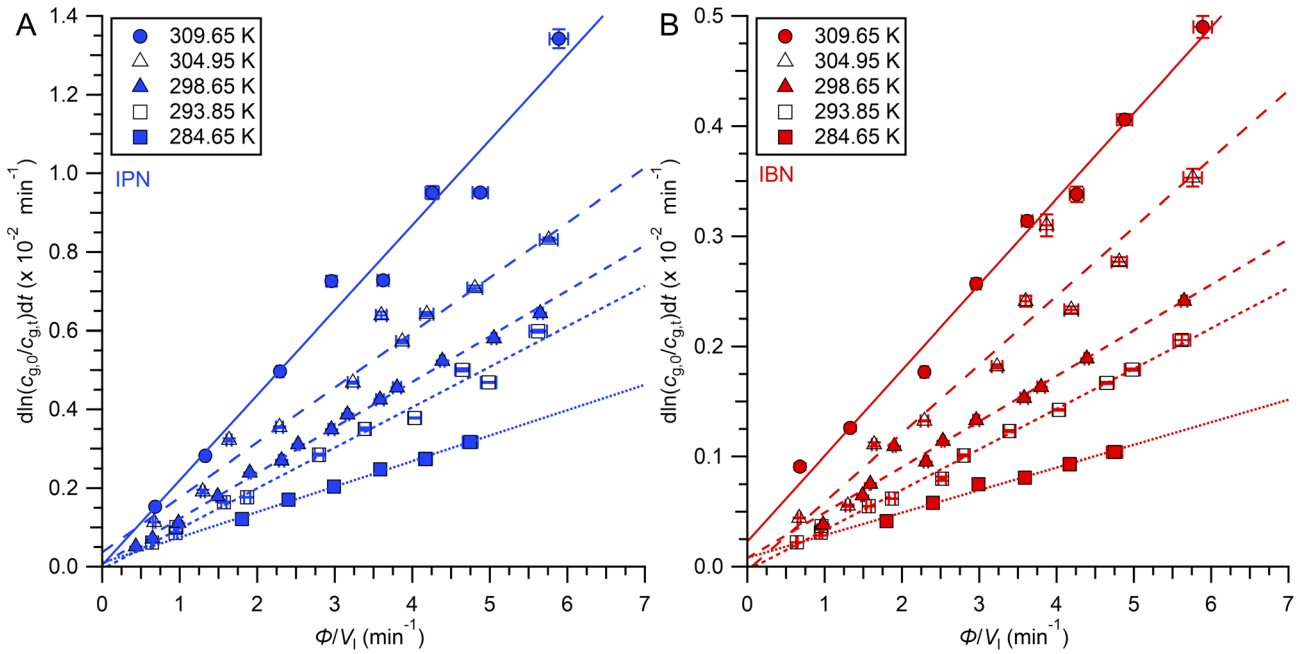

Fig. 3 Plots of $d\ln(c_{g,0}/c_{g,t})/dt$ *versus* Φ/V_l in *n*-octanol for IPN (panel A; blue colour) and IBN (panel B; red colour) at 309.65 K (●), 304.95 K (Δ), 298.65 K (▲), 293.85 K (□), and 284.65 K (■). The straight lines are linear fits to the data at each temperature. Error bars are ±1σ precision.

The Henry solubility is temperature dependent; that is, a compound is expected to partition from the liquid- to gas-phase more readily (*i.e.*, have a smaller H constant) at higher T. The temperature dependence of H constants measured in this work are described using a van't Hoff-type equation:[31]

$$\ln(H) = A_H - \frac{B_H}{T} + C_H \ln(T) \approx A_H - \frac{B_H}{T} \quad (5)$$

Values of A_H, B_H, and C_H were determined by least squares regression using Igor Pro software.

The Henry's law experiments were supplemented by estimates of H_{aq} and K_{OA} *via* bond contribution methods and quantitative structure–activity relationship models. A first set of estimates was obtained from the United States Environmental Protection Agency (EPA) Estimation Programs Interface (EPI) Suite v4.11, in which values of H_{aq} are predicted using the HENRYWIN v3.20 Bond Method described by Meylan and Howard,[32] and K_{OA} values are estimated using the KOAWIN v1.10 model.[33] The KOAWIN algorithm calculates K_{OA} according to eqn (2) using model-output estimates of K_{OW} and K_{AW} obtained by the KOWWIN v1.68 and HENRYWIN v3.20 models, respectively.[32–34] Additional predictions were obtained from the OPEn (Quantitative) Structure–activity/property Relationship App (OPERA)[35] v2.9 and the Iterative Fragment Selection Quantitative Structure–Activity Relationship (IFSQSAR)[36] python package v1.1.0 whose values were obtained *via* the Exposure And Safety Estimation (EAS-E) Suite website.[37] The latter also provides recommended, so-called "consensus", values that combine the plethora of quantitative structure property relationship predictions. The underlying theories and relative performances of each of these theoretical approaches have been discussed by Baskaran *et al.*[38] and Brown *et al.*[37]

3 Results

3.1 Octanol–air partitioning of IPN and IBN

The Henry's law solubility constants of IPN and IBN in *n*-octanol are summarized in Table 2. They are shown in the form of van't Hoff plots (*i.e.*, in logarithmic form plotted against 1000/T) in Fig. 4, alongside literature data for EN[12] and the EAS-E suite

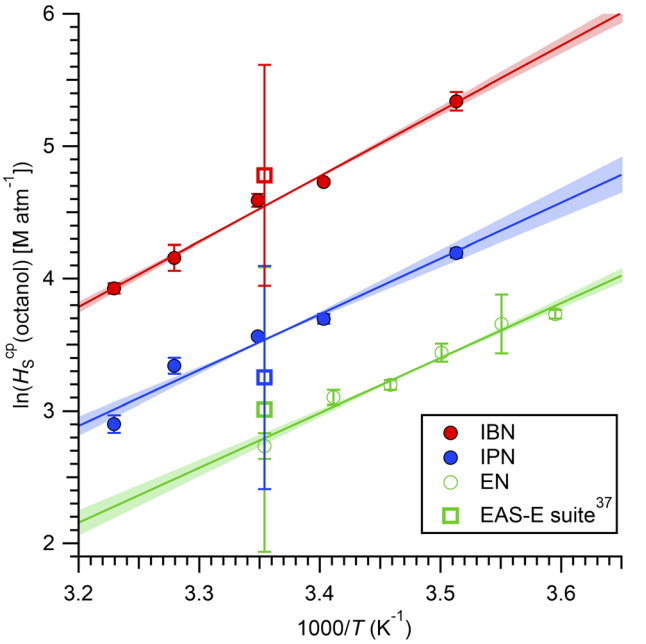

Fig. 4 Henry's law solubility constants of IBN (●, red colour) and IPN (●, blue colour) in *n*-octanol as functions of 1000/T. Ethyl nitrate data from Fig. 3 of Easterbrook *et al.*[12] are shown as open symbols (○, green colour). The EAS-E suite[37] consensus prediction values for K_{OA} of IBN (red), EN (green), and IPN (blue) at 298.15 K are represented as bolded squares (□). Fits to the data (Table 3) are shown as solid lines. The shaded regions represent upper and lower error bounds for each fit parameterization, *i.e.*, $\ln(H_{oct}) = (m + \sigma_m)10^3/T + (b - \sigma_b)$ and $\ln(H_{oct}) = (m - \sigma_m)\,10^3/T + (b + \sigma_b)$. Error bars are $\pm 1\sigma$ precision.

consensus value at 298.15 K. The H_{oct} values for IPN range from (18 ± 1) M atm^{-1} at 309.65 K to (66 ± 2) M atm^{-1} at 284.65 K. The H_{oct} values for IBN are larger than those of IPN, as expected from the bigger aliphatic side chain, and range from (51 ± 2) M atm^{-1} at 309.65 K to (208 ± 15) M atm^{-1} at 284.65 K.

Fits of the data shown in Fig. 4 to the full expression of eqn (5) in Igor Pro yielded C_H terms whose $\pm 1\sigma$ encompassed zero (not shown). Hence, the C_H term was omitted (*i.e.*, set to zero) in subsequent fits, and the simplified van't Hoff equation was instead used to parameterize the temperature dependence of H_{oct}

Table 2 Summary of experimental Henry's law solubility constants for EN, IPN, and IBN constants in *n*-octanol and deionized water (H_S^{cp} in M atm^{-1}). Uncertainties are at the $\pm 1\sigma$ level. n/d = not determined. The accuracy of the temperatures is ±0.5 K

	T (K)						
Compound and solvent	283.25	284.65	293.85	298.65	304.95	309.65	Reference
EN in *n*-octanol	38.8 ± 8.6 (281.7 K)	n/d	22.2 ± 1.3 (293.2 K)	15.4 ± 1.5 (298.2 K)	n/d	n/d	12
IPN in *n*-octanol	n/d	66 ± 2	40 ± 2	35.3 ± 0.5	28 ± 2	18 ± 1	This work
IBN in *n*-octanol	n/d	208 ± 15	113 ± 2	99 ± 5	64 ± 6	51 ± 2	This work
EN in DI water	3.98 ± 0.05 (281.7 K)	n/d	2.03 ± 0.06 (293.2 K)	1.56 ± 0.03 (298.2 K)	n/d	n/d	12
	4.09	3.73	2.07	1.54	1.07	0.82	14
IPN in DI water	2.41 ± 0.08	n/d	1.31 ± 0.04	0.92 ± 0.02	n/d	n/d	This work
	2.04	1.86	1.03	0.77	0.53	0.41	14
	1.18	1.10	0.69	0.54	0.41	0.33	39
IBN in DI water	n/d	n/d	0.87 ± 0.01	n/d	n/d	n/d	This work
	1.78	1.63	0.91	0.69	0.48	0.37	14

Table 3 Temperature dependence of Henry's law solubility constants for EN, IPN, and IBN. Uncertainties are at the ±1σ level. n/d = not disclosed. The variables ΔH^0_{soln} and ΔS^0_{soln} represent the enthalpy and entropy of solution, respectively

Compound and solvent	R^2 (%)	$-B_H$ (10^3 K)	A_H (unitless)	$-R \times B_H = \Delta H^0_{soln}$ (kJ mol^{-1})	$R \times A_H = \Delta S^0_{soln}$ (J K^{-1} mol^{-1})	Reference
EN in *n*-octanol	97.58	4.15 ± 0.33	−11.1 ± 1.9	34.5 ± 2.7	−92.4 ± 15.7	12
IPN in *n*-octanol	96.56	4.21 ± 0.46	−10.60 ± 1.54	35.0 ± 3.8	−88 ± 13	This work
IBN in *n*-octanol	99.22	4.94 ± 0.25	−12.01 ± 0.85	41.0 ± 2.1	−100 ± 7	This work
EN in DI water	99.24[a]	4.94 ± 0.11[a]	−16.2 ± 0.4[a]	41.1 ± 0.9[a]	−134.5 ± 3.3[a]	12 and 14
IPN in DI water	n/d	5.36 ± 0.09	−18.20 ± 0.36	44.53 ± 0.71	−151.3 ± 3	14
	98.4	4.30[b]	−19.63[b]	−35.8	−163.2	39
	99.52	5.19 ± 0.36	−17.43 ± 1.23	43.1 ± 3.0	−145 ± 10	This work
IBN in DI water	n/d	5.25 ± 0.15	−17.95 ± 0.48	43.62 ± 1.24	−149.2 ± 4	14

[a] EN data from Easterbrook *et al.*[12] combined with those of Kames and Schurath.[14] [b] Fit parameters listed in the Sander (2023) compilation.[5]

(and H_{aq}). The resulting fit parameters, *i.e.*, values of A_H and B_H, are summarized in Table 3, along with coefficient of determination (R^2) values. Based on the linear fits to the data in Fig. 4 (shown as solid lines), the H_{oct} data are best described by $\ln(H_S^{cp}(IPN)_{oct}/[M\ atm^{-1}]) = -(10.60 \pm 1.54) + (4214 \pm 459)/T$ and $\ln(H_S^{cp}(IBN)_{oct}/[M\ atm^{-1}]) = -(12.01 \pm 0.85) + (4937 \pm 253)/T$, where T is in kelvin (Table 3). The high linearity of the data in Fig. 4 corroborates the assumption that IPN and IBN achieve equilibrium within the bubble column.

3.2 Air-water partitioning of IPN and IBN

Van't Hoff plots summarizing the H_{aq} constants for IPN and IBN measured in this work are shown in Fig. 5A and B, respectively. Also shown are literature data from Kames and Schurath[14] (open circles) and Hauff *et al.*[39] (crosses) and the EAS-E suite consensus value (open squares). The Kames and Schurath parameterization[14] for IPN is currently recommended by the National Aeronautics and Space Administration Jet Propulsion Laboratory (NASA-JPL) Panel for Data Evaluation.[40]

The H_{aq} values for IPN measured in this work range from (0.92 ± 0.02) M atm^{-1} at 298.65 K to (2.41 ± 0.08) M atm^{-1} at 283.25 K and are best described by the expression $\ln(H_S^{cp}(IPN)_{aq}/[M\ atm^{-1}]) = -(17.43 \pm 1.23) + (5189 \pm 359)/T$ (Table 3). Overall, the solubility of IPN in DI water is lower (by a factor of ~40) than in *n*-octanol at each T.

For IPN, the data measured in this work are systematically larger (~20%, on average) than those of Kames and Schurath[14] and significantly larger than those of Hauff *et al.*[39] (*i.e.*, ~61%, on average). The H_{aq} data for IBN measured in this work are in good agreement with the data by Kames and Schurath.[14] The IBN data also demonstrate a lower solubility in DI water than in *n*-octanol, *i.e.*, its measured H_{aq} of (0.87 ± 0.01) M atm^{-1} at

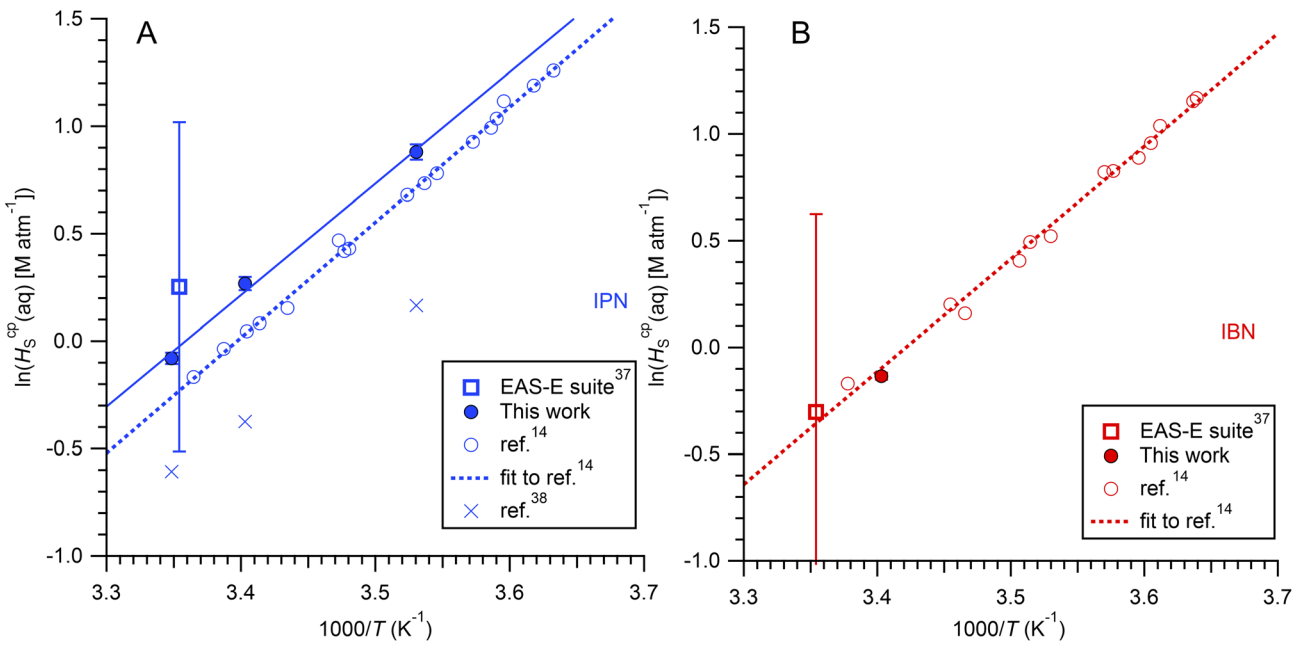

Fig. 5 Henry's law solubility constants of IPN (panel A, blue colour) and IBN (panel B, red colour) in DI water as functions of 1000/T. Data from this work are shown as solid circles (●) with a fit to the IPN data shown as a solid blue line. The EAS-E suite[37] consensus prediction values for IPN and IBN at 298.15 K are represented as bolded squares (□). The IPN and IBN data from Fig. 4 of Kames and Schurath[14] was extracted using "Engauge Digitizer" software[41] and are shown as open circles (○). The narrowly dashed lines (···) are linear fits to the extracted ("raw") data. Data calculated from the parameterization of Hauff *et al.*[39] are shown as cross symbols (×). Error bars are ±1σ precision.

Table 4 Experimental octanol–water partition coefficients (K_{OW}) of EN, IPN, and IBN. Uncertainties are at the $\pm 1\sigma$ level. n/d = not determined. The accuracy of the temperatures is ±0.5 K

	T (K)						
Compound	283.25	284.65	293.85	298.65	304.95	309.65	Ref.
EN	—	—	11.0 ± 0.7	9.9 ± 1.0	—	—	12[a]
	—	—	10.3 ± 0.6	9.7 ± 1.0	—	—	12[b]
IPN	30 ± 1	n/d	31 ± 2	38 ± 1	n/d	n/d	[a]
	n/d	36 ± 1	39 ± 1	46 ± 1	53 ± 3	45 ± 3	[b]
IBN	n/d	n/d	129 ± 3	n/d	n/d	n/d	[a]
	n/d	128 ± 9	124 ± 2	144 ± 7	134 ± 13	138 ± 5	[b]

[a] Calculated using H_{aq} and H_{oct} values determined by this group. [b] Calculated using H_{aq} values from Kames and Schurath[14] and H_{oct} values determined by this group.

293.85 K is a factor of (130 ± 3) smaller than its H_{oct} at the same T.

3.3 Octanol–water partitioning of IPN, IBN and EN

Octanol–water partition coefficients of IPN and IBN, calculated *via* eqn (2) using H_{oct} and H_{aq} values measured in this work, are summarized in Table 4 and Fig. S3 (solid circles). The K_{OW} values are (33 ± 5) for IPN and (1.3 ± 0.1) × 10^2 for IBN on average; both are larger than the K_{OW} values for EN (Table 4) and increase with the size of the aliphatic side chain as one would expect.

For IPN, K_{OW} values derived solely from H constants measured in this work are smaller, by factors of ∼1.26 and ∼1.21 at 293.85 K and 298.65 K, respectively, than those calculated with H_{oct} values from this work and H_{aq} values from Kames and Schurath[14] (Table 4; shown as open circles in Fig. S3). For IBN, in contrast, the K_{OW} values calculated by both methods are consistent with each other, *i.e.*, at 293.85 K, a K_{OW} value of (129 ± 3) is calculated using H_{oct} and H_{aq} measured in this work, which agrees with the value of (124 ± 2) calculated using H_{aq} values from Kames and Schurath.[14] This result is not surprising as the respective H_{aq} values agree well (∼0.9 M atm^{-1}).

Using either calculation method, the K_{OW} values for both IPN and IBN exhibit a T dependence between 284.65 K and 309.65 K. Linear fits of ln(K_{OW}(IPN)) *versus* 1000/T (Fig. S3) yielded ln(K_{OW}(IPN)) = ((−1.15 ± 0.84) K) × (1000/T) + (7.4 ± 2.8), R^2 = 0.65 when using H_{aq} data from this work and ln(K_{OW}(IPN)) = ((−1.14 ± 0.46) K) × (1000/T) + (7.6 ± 1.5), R^2 = 0.67 when using H_{aq} data from Kames and Schurath.[14] The IBN data also display a T dependence best described by ln(K_{OW}(IBN)) = ((−0.31 ± 0.25) K) × (1000/T) + (5.93 ± 0.85), R^2 = 0.33. Attempts to increase the range of T studied (*e.g.*, to conduct experiments at T = 318 K) were thwarted by decay kinetics which was too fast for GC analysis along with issues arising from evaporation and condensation of *n*-octanol or water in the transfer tubing.

The results for IPN and IBN prompted us to re-examine our earlier reported K_{OW} values for EN,[12] listed in Table 4 and shown graphically in Fig. S3 (solid green circles). Consistent with the IBN results from this work, the K_{OW} for EN show a weak T dependence (R^2 = 0.44) when calculated using H_{oct} and H_{aq} values measured by this group. However, a stronger T dependence (R^2 = 0.77) emerges when K_{OW} values are calculated using H_{aq} values by Kames and Schurath[14] (shown as open circles and in black colour in Fig. S3), suggesting a small but systematic bias between the two data sets.

3.4 Liquid phase loss rates of IPN and IBN

Beyond partitioning, the analytes may, in principle, be removed by chemical reactions (*e.g.*, hydrolysis or thermal degradation) within the liquid phase. The pseudo-first order rate constants for such liquid-phase losses (k_1) were derived from the y-intercepts of plots shown in Fig. 3 (*n*-octanol) and S2 (DI water) and are summarized in Table S6. Their values were uniformly small, *i.e.*, <10^{-4} s^{-1} (at the 95% confidence level) for both IPN and IBN and in either octanol or water. Further, within the measurement uncertainty, the k_l values of IPN and IBN often encompassed zero. This suggests that liquid-phase losses (beyond partitioning) were negligible under our experimental conditions.

4 Discussion

This work represents the first (and only) experimental determination of H_{oct} for IPN and IBN (to the best of our knowledge). The measured H_{oct} constants for IBN are larger than those of IPN, which are in turn larger than those of EN, previously determined by our group.[12] The trend is rationalized by the relative aliphatic side chain lengths of each compound, *i.e.*, the solubility of ANs in *n*-octanol is proportional to the number of carbon atoms present in the alkyl chain. For example, at 298 K the H_{oct} of IBN (four C atoms) is ∼2.8× larger than that of IPN (three C atoms), which is in turn a factor of ∼2.3 larger than that of EN (two C atoms) (Table 2), as one might expect.

The experimental H_{oct} and K_{OA} values are in quantitative agreement with IFSQSAR predictions (Table 5), though it appears that the model's uncertainty estimates are perhaps too conservative (*i.e.*, the model is performing better than its own algorithm's error analysis suggests). In contrast, predictions by the older OPERA and EPI suite models are less accurate. For example, the KOAWIN model overestimates the experimental K_{OA} values for EN and IBN at 298 K by factors of ∼4.4 and ∼3.2, respectively (Table 5). Predictions of K_{OA} by the OPERA model

Table 5 Experimental H_S^{cp}, K_{OA}, and K_{OW} values for EN, IPN, and IBN at 298 K and their corresponding predicted values by the EPI suite, OPERA, and IFSQSAR models as well as the EAS-E suite consensus value.[33–37] Uncertainties are at the $\pm 1\sigma$ level

	H_S^{cp}(oct) (M atm^{-1})			H_S^{cp}(aq) (M atm^{-1})			K_{OA}			K_{OW}		
	EN	IPN	IBN	EN	IPN	IBN[14]	EN	IPN	IBN	EN	IPN	IBN
EPI suite	68	28	311	3.79	2.86	2.16	1656	3192	7621	17.8	45.7	144.5
OPERA	9 ± 4	20 ± 5	76 ± 27	1.63 ± 0.07	0.62 ± 0.04	0.45 ± 0.03	209 ± 101	501 ± 115	1862 ± 665	0.01 ± 0.04	0.2 ± 1.1	5.1 ± 24.1
IFSQSAR	15 ± 7	30 ± 27	71 ± 65	1.55 ± 0.07	1.2 ± 4.0	0.42 ± 1.40	355 ± 163	724 ± 667	1738 ± 1601	14.5 ± 7.0	36.3 ± 76.9	204 ± 437
Consensus	20 ± 22	26 ± 22	119 ± 99	2.1 ± 1.1	1.3 ± 1.0	0.74 ± 0.69	497 ± 534	632 ± 128	2911 ± 2426	16.0 ± 2.4	40.7 ± 6.7	53 ± 109
Experiment	15.4 ± 1.5	35.3 ± 0.5	99 ± 5	1.56 ± 0.03	0.92 ± 0.02	0.69[a]	380 ± 35[b]	863 ± 14[c]	2400 ± 110[c]	9.9 ± 1.0[b]	46 ± 1[c]	144 ± 7[c]

[a] Value from Kames and Schurath.[14] [b] Calculated using H_{aq} and H_{oct} values determined by this group.[12] [c] Calculated using H_{aq} values from Kames and Schurath[14] and H_{oct} values determined by this group.

are likewise in poor agreement with experimental EN and IPN data, though are more accurate for IBN. It hence stands to reason that OPERA and KOAWIN would err with respect to the polarity of the nitrate moiety (–ONO_2) in general, hampering their ability to accurately predict properties of higher molecular weight ANs such as terpene nitrates which are challenging to synthesize.[42] Considering the relatively large biases of EPI Suite and OPERA, it may be advised to re-examine how the recommended "consensus" values are calculated for these compounds within EAS-E suite, as the arithmetic average of the three models is less accurate than the IFSQSAR model on its own.

The H_{oct} values measured in this work are useful in that they allow calculation of K_{OW} for IPN and IBN, though this calculation requires accurate values of H_{aq}. Whereas experimental values for IPN have been reported by two groups,[14,39] with the study by Kames and Schurath[14] recommended by the National Aeronautics and Space Administration Jet Propulsion Laboratory (NASA-JPL) evaluation panel,[40] the work by Kames and Schurath[14] is the only experimental study reporting H_{aq} values for IBN. Because of the low number of H_{aq} measurements for IPN and IBN and the earlier discovered[12] erroneous parameterization for EN in Kames and Schurath,[14] corroboration was warranted.

Our H_{aq} data (Fig. 5) are in reasonable agreement with those by Kames and Schurath,[14] ~20% larger for IPN and ~4% lower for IBN (Table 2) and with the same temperature dependence (Table 3) for IPN. Our data do not agree with the measurements by Hauff *et al.*,[39] whose data are ~40% to ~50% lower than ours. We are unsure why our H_{aq} data for IPN would differ from the Kames and Schurath H_{aq} data,[14] considering that our EN and IBN data agree within ±2% and ±4% respectively, which eliminates by-and-large the possibility of experimental error (such as an incorrect temperature calibration). A possible reason for a discrepancy between the H_{aq} data to occur for one compound, but not others, would be the presence of an impurity such as nitric acid (HNO_3), a potential side product of the synthesis from N_2O_5, or residual alcohol reagent. The presence of HNO_3 would suppress the solubility due to the Setschenow effect,[43] whereas the presence of alcohol would increase it. For IPN, though, both studies used a commercial sample with ≥99% purity, such that the reason for the discrepancy between the H_{aq} data remains unclear. In contrast, the H_{oct} values were measured using commercial IPN and IBN samples, *i.e.*, would not have been affected by impurities. Encouragingly, the experimental H_{aq} values agree reasonably well (within ±30%) with the predictions by OPERA and IFSQSAR, though not the HENRYWIN model which considerably overestimates H_{aq} for EN, IPN, and IBN (Table 5) by factors of two to three.

The K_{OW} values, calculated using both our and the Kames and Schurath[14] data to err on the side of caution (Table 4 and Fig. S3), are in reasonable agreement with IFSQSAR and KOWWIN though not with OPERA model predictions which are inexplicably off by more than one order of magnitude. Even though the ANs studied in this work do not exhibit a large K_{OW}, and the discrepancy between models and experiment is not consequential for these compounds, it may likely be of importance for K_{OW} predictions of larger, multifunctional ANs that are present in the organic aerosol phase.[44–46]

4.1 Atmospheric implications

Laboratory[44] and field[45,46] studies have shown that alkyl and multifunctional nitrates can comprise a large mass fraction of SOA, with the chemical processing of monoterpene- and isoprene-derived nitrates thought to contribute significantly to the formation of particulate $RONO_2$ within organic and aqueous aerosol.[47] In particular, the nitrate radical (NO_3) oxidation of monoterpenes (*e.g.*, α- and β-pinene) has been identified as a dominant SOA source in monoterpene-rich environments.[3,48] Simulations of SOA formation from these and other VOC precursors have traditionally relied on SOA mass yield data, which are often derived from gas/aerosol partitioning models.[49] Atmospheric models also assume that the formation of SOA species from individual VOCs are independent,[50] and that mass yields from individual VOC precursors are linearly additive, though this notion has recently been challenged by Takeuchi *et al.*[51] Considering current approaches to SOA simulations and assumptions made by atmospheric models, it is clear that accurate values of K_{OA} and H_{aq} for key SOA precursors (*i.e.*,

monoterpene and isoprene nitrates)[52,53] are essential to correctly describe their partition behaviour and SOA formation potential. Unfortunately, experimental determination of these parameters for monoterpene- and isoprene nitrates is largely inaccessible, hence knowledge of their partitioning is heavily dependent on SAR estimates. In this context, the inconsistent and inaccurate predictions by KOAWIN and HENRYWIN for ANs, and organic nitrates more broadly, carry significant implications for modelling the formation and fate of particulate $RONO_2$ in condensed phases. Since hydrolysis of particulate $RONO_2$ in the condensed phase is thought to represent a sink of atmospheric NO_x,[47] such inaccuracies further affect our understanding of NO_x cycling in the troposphere. In addition, long-term exposure to SOA has been linked to increased cardiorespiratory mortality,[54] further underscoring the need for accurate partitioning parameters to improve predictions of both atmospheric processes and health impacts of SOA.

5 Conclusions

This study provides the first experimental determination of K_{OA} and K_{OW} for IPN and IBN at atmospherically relevant temperatures. The data narrow a significant knowledge gap considering the paucity of experimental K_{OA} and K_{OW} data for organic nitrates overall. Estimates by the KOAWIN and HENRYWIN models were inconsistent with experimental measurements of K_{OA} and K_{AW} for IPN and IBN reported in this work, which is not surprising considering KOAWIN has been demonstrated to be more poorly performing than other prediction techniques.[38] On the other hand, predictions by the IFSQSAR model were consistent with experiment, though the experimental data may now be used to reduce this model's overly generous uncertainty estimates. Additional experimental measurements are needed for other short chain ANs to help improve the predictability of models for this chemical class. Namely, data for methyl nitrate would corroborate the potential under-expression of the nitrate group observed with small molecules (*i.e.*, overestimation of EN) and data for larger ANs (*e.g.*, n-propyl, *n*-butyl and *n*-pentyl nitrate) will corroborate the differences observed for IPN and IBN in this work.

Author contributions

HDO conceptualized the experiments. AJB, VKL and KDE carried out the experiments and reduced the data. DNI synthesized N_2O_5 and IBN. AJB and KDE drafted the manuscript with input from HDO and NS. KDE prepared the figures, including the table of contents figure.

Conflicts of interest

The authors declare that they have no conflict of interest.

Data availability

Data supporting the laboratory experiments described in this article have been included as part of the supplementary information (SI). Supplementary information: 3 figures and 6 tables, including a schematic of the bubble column apparatus (Fig. S1), the experimental schedules (Tables S1–S3), dimensionless Henry's law constants (Table S5) and liquid phase loss rate constants (Table S6). See DOI: https://doi.org/10.1039/d5em00940e.

Acknowledgements

This work was made possible by the financial support of the Natural Sciences and Engineering Research Council of Canada (NSERC) in the form of a Discovery grant to HDO (RGPIN-2022-03128) and CGS-M scholarship to KDE. VKL acknowledges financial support from the University of Calgary's Program for Undergraduate Research Experience (PURE). Article processing charges for open access publishing of this work were paid *via* an institutional agreement by the Canadian Research Knowledge Network.

References

1 D. K. Farmer, A. E. Perring, P. J. Wooldridge, D. R. Blake, A. Baker, S. Meinardi, L. G. Huey, D. Tanner, O. Vargas and R. C. Cohen, Impact of organic nitrates on urban ozone production, *Atmos. Chem. Phys.*, 2011, **11**, 4085–4094.
2 M. R. Beaver, J. M. S. Clair, F. Paulot, K. M. Spencer, J. D. Crounse, B. W. LaFranchi, K. E. Min, S. E. Pusede, P. J. Wooldridge, G. W. Schade, C. Park, R. C. Cohen and P. O. Wennberg, Importance of biogenic precursors to the budget of organic nitrates: observations of multifunctional organic nitrates by CIMS and TD-LIF during BEARPEX 2009, *Atmos. Chem. Phys.*, 2012, **12**, 5773–5785.
3 A. Kiendler-Scharr, A. A. Mensah, E. Friese, D. Topping, E. Nemitz, A. S. H. Prevot, M. Aijala, J. Allan, F. Canonaco, M. Canagaratna, S. Carbone, M. Crippa, M. Dall Osto, D. A. Day, P. De Carlo, C. F. Di Marco, H. Elbern, A. Eriksson, E. Freney, L. Hao, H. Herrmann, L. Hildebrandt, R. Hillamo, J. L. Jimenez, A. Laaksonen, G. McFiggans, C. Mohr, C. O'Dowd, R. Otjes, J. Ovadnevaite, S. N. Pandis, L. Poulain, P. Schlag, K. Sellegri, E. Swietlicki, P. Tiitta, A. Vermeulen, A. Wahner, D. Worsnop and H. C. Wu, Ubiquity of organic nitrates from nighttime chemistry in the European submicron aerosol, *Geophys. Res. Lett.*, 2016, **43**, 7735–7744.
4 R. Sander, W. E. Acree, A. De Visscher, S. E. Schwartz and T. J. Wallington, Henry's law constants (IUPAC Recommendations 2021), *Pure Appl. Chem.*, 2022, **94**, 71–85.
5 R. Sander, Compilation of Henry's law constants (version 5.0.0) for water as solvent, *Atmos. Chem. Phys.*, 2023, **23**, 10901–12440.
6 S. Baskaran, Y. D. Lei and F. Wania, A Database of Experimentally Derived and Estimated Octanol–Air Partition Ratios (K_{OA}), *Journal of Physical and Chemical Reference Data*, 2021, **50**, 043101.
7 J. M. Parnis and D. Mackay, *Multimedia Environmental Models: the Fugacity Approach*, Taylor & Francis, 3rd edn, 2020.

8 J. M. Roberts, The atmospheric chemistry of organic nitrates, *Atmos. Environm. A*, 1990, **24**, 243–287.
9 K. Treves, L. Shragina and Y. Rudich, Measurement of octanol-air partition coefficients using solid-phase microextraction (SPME) - application to hydroxy alkyl nitrates, *Atmos. Environm.*, 2001, **35**, 5843–5854.
10 J. M. Roberts, Measurement of the Henry's law coefficient and first order loss rate of PAN in n-octanol, *Geophys. Res. Lett.*, 2005, **32**, L08803.
11 K. D. Easterbrook, M. A. Vona, K. Nayebi-Astaneh, A. M. Miller and H. D. Osthoff, Measurement of Henry's law and liquid-phase loss rate constants of peroxypropionic nitric anhydride (PPN) in deionized water and in n-octanol, *Atmos. Chem. Phys.*, 2023, **23**, 311–322.
12 K. D. Easterbrook, M. A. Vona and H. D. Osthoff, Measurement of Henry's law constants of ethyl nitrate in deionized water, synthetic sea salt solutions, and n-octanol, *Chemosphere*, 2024, **346**, 140482.
13 C. Hansch and A. Leo, *Substituent Constants for Correlation Analysis in Chemistry and Biology*, Wiley, 1979.
14 J. Kames and U. Schurath, Alkyl nitrates and bifunctional nitrates of atmospheric interest - Henry Law Constants and their temperature dependencies, *J. Atmos. Chem.*, 1992, **15**, 79–95.
15 R. G. Fischer and K. Ballschmiter, Determination of vapor pressure, water solubility, gas-water partition coefficient P_{GW}, Henry's law constant, and octanol-water partition coefficient P_{OW} of 26 alkyl dinitrates, *Chemosphere*, 1998, **36**, 2891–2901.
16 R. G. Fischer and K. Ballschmiter, Prediction of the environmental distribution of alkyl dinitrates – Chromatographic determination of vapor pressure p_0, water solubility $S(H_2O)$, gas-water partition coefficient K_{GW} (Henry's law constant) and octanol-water partition coefficient K_{OW}, *Fresenius Journal of Analytical Chemistry*, 1998, **360**, 769–776.
17 J. Sangster, Octanol-Water Partition Coefficients of Simple Organic Compounds, *Journal of Physical and Chemical Reference Data*, 1989, **18**, 1111–1229.
18 D. Mackay, W. Y. Shiu, K.-C. Ma and S. C. Lee, *Handbook of Physical-Chemical Properties and Environmental Fate for Organic Chemicals*, CRC/Taylor & Francis, Boca Raton, FL, 2nd edn, 2006.
19 T. Raventos-Duran, M. Camredon, R. Valorso, C. Mouchel-Vallon and B. Aumont, Structure-activity relationships to estimate the effective Henry's law constants of organics of atmospheric interest, *Atmos. Chem. Phys.*, 2010, **10**, 7643–7654.
20 L. Xu, H. O. T. Pye, J. He, Y. Chen, B. N. Murphy and N. L. Ng, Experimental and model estimates of the contributions from biogenic monoterpenes and sesquiterpenes to secondary organic aerosol in the southeastern United States, *Atmos. Chem. Phys.*, 2018, **18**, 12613–12637.
21 S. B. Bertman, J. M. Roberts, D. D. Parrish, M. P. Buhr, P. D. Goldan, W. C. Kuster, F. C. Fehsenfeld, S. A. Montzka and H. Westberg, Evolution of alkyl nitrates with air mass age, *J. Geophys. Res.*, 1995, **100**, 22805–22813.
22 H. Sun, D. Gu, Z. Xu, X. Feng, X. Cao, Y. Mai, X. Li, H. W. Lee, K. F. Leung, T. C. Tse, W. M. Chan and S. K. Mak, Seasonal variation and origins of C1–C5 alkyl nitrates: A year-long study at a Hong Kong coastal site, *Atmos. Environm.*, 2024, **338**, 120824.
23 J. M. González-Sánchez, N. Brun, J. Wu, S. Ravier, J. L. Clément and A. Monod, On the importance of multiphase photolysis of organic nitrates on their global atmospheric removal, *Atmos. Chem. Phys.*, 2023, **23**, 5851–5866.
24 J.-C. Lerol, J.-C. Masson, H. Renon, J.-F. Fabries and H. Sannier, Accurate Measurement of Activity Coefficient at Infinite Dilution by Inert Gas Stripping and Gas Chromatography, *Industrial & Engineering Chemistry Process Design and Development*, 1977, **16**, 139–144.
25 N. D. Rider, Y. M. Taha, C. A. Odame-Ankrah, J. A. Huo, T. W. Tokarek, E. Cairns, S. G. Moussa, J. Liggio and H. D. Osthoff, Efficient photochemical generation of peroxycarboxylic nitric anhydrides with ultraviolet light-emitting diodes, *Atmos. Meas. Tech.*, 2015, **8**, 2737–2748.
26 J. Kames, U. Schurath, F. Flocke and A. Volzthomas, Preparation of organic nitrates from alcohols and N_2O_5 for species identification in atmospheric samples, *J. Atmos. Chem.*, 1993, **16**, 349–359.
27 J. A. Davidson, A. A. Viggiano, C. J. Howard, I. Dotan, F. C. Fehsenfeld, D. L. Albritton and E. E. Ferguson, Rate Constants For Reactions Of O_2^+, NO_2^+, NO^+, H_3O^+, CO_3^-, NO_2^-, And Halide Ions With N_2O_5 At 300 K, *J. Chem. Phys.*, 1978, **68**, 2085–2087.
28 C. A. Odame-Ankrah and H. D. Osthoff, A compact diode laser cavity ring-down spectrometer for atmospheric measurements of NO_3 and N_2O_5 with automated zeroing and calibration, *Appl. Spectrosc.*, 2011, **65**, 1260–1268.
29 J. Kames and U. Schurath, Henry's law and hydrolysis rate constants for peroxyacyl nitrates (PANs) using a homogeneous gas-phase source, *J. Atmos. Chem.*, 1995, **21**, 151–164.
30 T. W. Tokarek, J. A. Huo, C. A. Odame-Ankrah, D. Hammoud, Y. M. Taha and H. D. Osthoff, A gas chromatograph for quantification of peroxycarboxylic nitric anhydrides calibrated by thermal dissociation cavity ring-down spectroscopy, *Atmos. Meas. Tech.*, 2014, **7**, 3263–3283.
31 J. Staudinger and P. V. Roberts, A critical compilation of Henry's law constant temperature dependence relations for organic compounds in dilute aqueous solutions, *Chemosphere*, 2001, **44**, 561–576.
32 W. M. Meylan and P. H. Howard, Bond contribution method for estimating Henry's law constants, *Environmental Toxicology and Chemistry*, 1991, **10**, 1283–1293.
33 W. M. Meylan and P. H. Howard, Estimating octanol–air partition coefficients with octanol–water partition coefficients and Henry's law constants, *Chemosphere*, 2005, **61**, 640–644.
34 W. M. Meylan and P. H. Howard, Atom/fragment contribution method for estimating octanol–water partition coefficients, *J. Pharm. Sci.*, 1995, **84**, 83–92.

35 K. Mansouri, C. M. Grulke, R. S. Judson and A. J. Williams, OPERA models for predicting physicochemical properties and environmental fate endpoints, *J. Cheminf.*, 2018, **10**, 10.
36 T. N. Brown, A. Sangion and J. A. Arnot, Identifying uncertainty in physical-chemical property estimation with IFSQSAR, *J. Cheminf.*, 2024, **16**, 65.
37 T. N. Brown, A. Sangion, L. Li and J. A. Arnot, Quantifying uncertainty in predicted chemical partition ratios required for chemical assessments, *Environ. Sci.: Processes Impacts*, 2025, **27**, 3457–3470.
38 S. Baskaran, Y. D. Lei and F. Wania, Reliable Prediction of the Octanol–Air Partition Ratio, *Environ. Toxicol. Chem.*, 2021, **40**, 3166–3180.
39 K. Hauff, R. G. Fischer and K. Ballschmiter, Determination of C-1-C-5 alkyl nitrates in rain, snow, white frost, lake, and tap water by a combined codistillation head-space gas chromatography technique. Determination of Henry's law constants by head-space GC, *Chemosphere*, 1998, **37**, 2599–2615.
40 J. B. Burkholder, S. P. Sander, J. P. D. Abbatt, J. R. Barker, C. Cappa, J. D. Crounse, T. S. Dibble, R. E. Huie, C. E. Kolb, M. J. Kurylo, V. L. Orkin, C. J. Percival, D. M. Wilmouth and P. H. Wine, *Chemical Kinetics and Photochemical Data for Use in Atmospheric Studies, Evaluation Number 19*, National Aeronautics and Space Administration, Jet Propulsion Laboratory, California Institute of Technology, Pasadena, California, 2020.
41 M. Mitchell, *Engauge Digitizer*, 2020, DOI: 10.5281/zenodo.3941227.
42 E. A. McKnight, N. P. Kretekos, D. Owusu and R. L. LaLonde, Technical note: Preparation and purification of atmospherically relevant α-hydroxynitrate esters of monoterpenes, *Atmos. Chem. Phys.*, 2020, **20**, 4241–4254.
43 J. Setschenow, Über die Konstitution der Salzlösungen auf Grund ihres Verhaltens zu Kohlensäure, *Zeitschrift für Physikalische Chemie*, 1889, **4U**, 117–125.
44 B. Brownwood, A. Turdziladze, T. Hohaus, R. Wu, T. F. Mentel, P. T. M. Carlsson, E. Tsiligiannis, M. Hallquist, S. Andres, L. Hantschke, D. Reimer, F. Rohrer, R. Tillmann, B. Winter, J. Liebmann, S. S. Brown, A. Kiendler-Scharr, A. Novelli, H. Fuchs and J. L. Fry, Gas-Particle Partitioning and SOA Yields of Organonitrate Products from NO3-Initiated Oxidation of Isoprene under Varied Chemical Regimes, *ACS Earth Space Chem.*, 2021, **5**, 785–800.
45 A. W. Rollins, E. C. Browne, K.-E. Min, S. E. Pusede, P. J. Wooldridge, D. R. Gentner, A. H. Goldstein, S. Liu, D. A. Day, L. M. Russell and R. C. Cohen, Evidence for NO_x Control over Nighttime SOA Formation, *Science*, 2012, **337**, 1210–1212.
46 R. A. Zaveri, J. E. Shilling, J. D. Fast and S. R. Springston, Efficient Nighttime Biogenic SOA Formation in a Polluted Residual Layer, *J. Geophys. Res.-Atmos.*, 2020, **125**, e2019JD031583.
47 A. Zare, K. M. Fahey, G. Sarwar, R. C. Cohen and H. O. T. Pye, Vapor-Pressure Pathways Initiate but Hydrolysis Products Dominate the Aerosol Estimated from Organic Nitrates, *ACS Earth Space Chem.*, 2019, **3**, 1426–1437.
48 L. Xu, H. Guo, C. M. Boyd, M. Klein, A. Bougiatioti, K. M. Cerully, J. R. Hite, G. Isaacman-VanWertz, N. M. Kreisberg, C. Knote, K. Olson, A. Koss, A. H. Goldstein, S. V. Hering, J. de Gouw, K. Baumann, S.-H. Lee, A. Nenes, R. J. Weber and N. L. Ng, Effects of anthropogenic emissions on aerosol formation from isoprene and monoterpenes in the southeastern United States, *Proc. Natl. Acad. Sci.*, 2015, **112**, 37–42.
49 J. F. Pankow, An absorption model of gas-particle partitioning of organic compounds in the atmosphere, *Atmos. Environm.*, 1994, **28**, 185–188.
50 K. W. Appel, S. L. Napelenok, K. M. Foley, H. O. T. Pye, C. Hogrefe, D. J. Luecken, J. O. Bash, S. J. Roselle, J. E. Pleim, H. Foroutan, W. T. Hutzell, G. A. Pouliot, G. Sarwar, K. M. Fahey, B. Gantt, R. C. Gilliam, N. K. Heath, D. Kang, R. Mathur, D. B. Schwede, T. L. Spero, D. C. Wong and J. O. Young, Description and evaluation of the Community Multiscale Air Quality (CMAQ) modeling system version 5.1, *Geosci. Model Dev.*, 2017, **10**, 1703–1732.
51 M. Takeuchi, T. Berkemeier, G. Eris and N. L. Ng, Non-linear effects of secondary organic aerosol formation and properties in multi-precursor systems, *Nat. Commun.*, 2022, **13**, 7883.
52 N. L. Ng, A. J. Kwan, J. D. Surratt, A. W. H. Chan, P. S. Chhabra, A. Sorooshian, H. O. T. Pye, J. D. Crounse, P. O. Wennberg, R. C. Flagan and J. H. Seinfeld, Secondary organic aerosol (SOA) formation from reaction of isoprene with nitrate radicals (NO_3), *Atmos. Chem. Phys.*, 2008, **8**, 4117–4140.
53 H. O. T. Pye, A. W. H. Chan, M. P. Barkley and J. H. Seinfeld, Global modeling of organic aerosol: the importance of reactive nitrogen (NO_x and NO_3), *Atmos. Chem. Phys.*, 2010, **10**, 11261–11276.
54 H. O. T. Pye, C. K. Ward-Caviness, B. N. Murphy, K. W. Appel and K. M. Seltzer, Secondary organic aerosol association with cardiorespiratory disease mortality in the United States, *Nat. Commun.*, 2021, **12**, 7215.